Wetting considerations in capillary rise and imbibition in closed square tubes and open rectangular cross-section channels

F. Fouzia Ouali, Glen McHale, Haadi Javed, Christophe Trabi, Neil J. Shirtcliffe & Michael I. Newton

Microfluidics and Nanofluidics

ISSN 1613-4982
Volume 15
Number 3

Microfluid Nanofluid (2013) 15:309-326
DOI 10.1007/s10404-013-1145-5

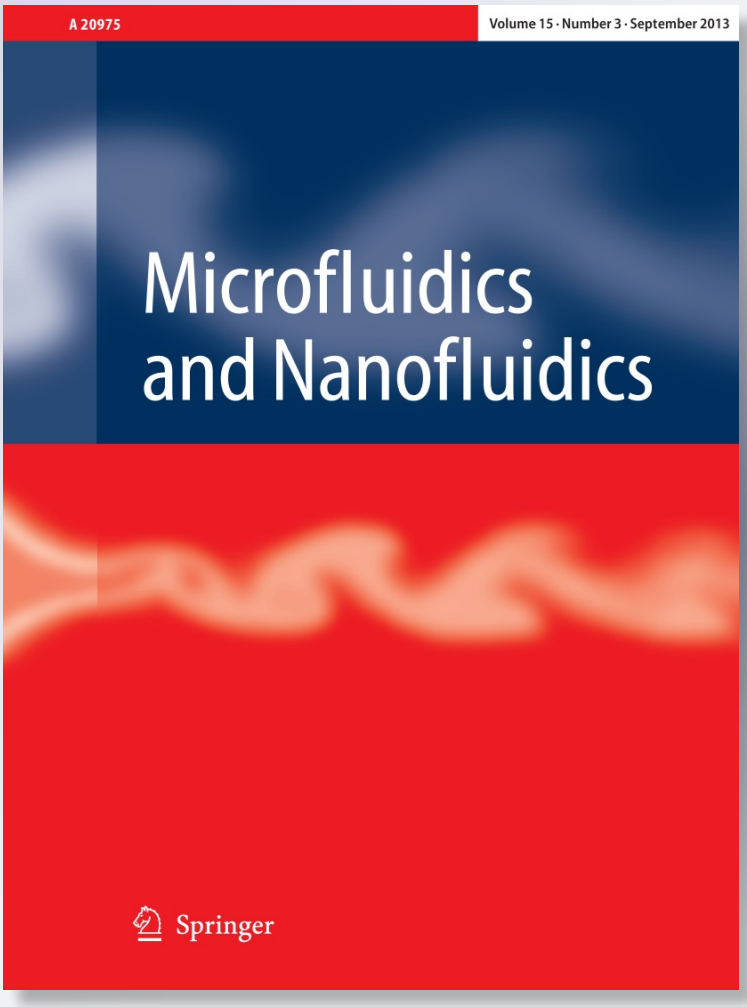

Springer

Microfluid Nanofluid (2013) 15:309–326
DOI 10.1007/s10404-013-1145-5

RESEARCH PAPER

Wetting considerations in capillary rise and imbibition in closed square tubes and open rectangular cross-section channels

F. Fouzia Ouali · Glen McHale · Haadi Javed · Christophe Trabi · Neil J. Shirtcliffe · Michael I. Newton

Received: 1 August 2012 / Accepted: 17 January 2013 / Published online: 13 February 2013

Abstract The spontaneous capillary-driven filling of microchannels is important for a wide range of applications. These channels are often rectangular in cross-section, can be closed or open, and horizontal or vertically orientated. In this work, we develop the theory for capillary imbibition and rise in channels of rectangular cross-section, taking into account rigidified and non-rigidified boundary conditions for the liquid–air interfaces and the effects of surface topography assuming Wenzel or Cassie-Baxter states. We provide simple interpolation formulae for the viscous friction associated with flow through rectangular cross-section channels as a function of aspect ratio. We derive a dimensionless cross-over time, T_c, below which the exact numerical solution can be approximated by the Bousanquet solution and above which by the visco-gravitational solution. For capillary rise heights significantly below the equilibrium height, this cross-over time is $T_c \approx (3X_e/2)^{2/3}$ and has an associated dimensionless cross-over rise height $X_c \approx (3X_e/2)^{1/3}$, where $X_e = 1/G$ is the dimensionless equilibrium rise height and G is a dimensionless form of the acceleration due to gravity. We also show from wetting considerations that for rectangular channels, fingers of a wetting liquid can be expected to imbibe in advance of the main meniscus along the corners of the channel walls. We test the theory via capillary rise experiments using polydimethylsiloxane oils of viscosity 96.0, 48.0, 19.2 and 4.8 mPa s within a range of closed square tubes and open rectangular cross-section channels with SU-8 walls. We show that the capillary rise heights can be fitted using the exact numerical solution and that these are similar to fits using the analytical visco-gravitational solution. The viscous friction contribution was found to be slightly higher than predicted by theory assuming a non-rigidified liquid–air boundary, but far below that for a rigidified boundary, which was recently reported for imbibition into horizontally mounted open microchannels. In these experiments we also observed fingers of liquid spreading along the internal edges of the channels in advance of the main body of liquid consistent with wetting expectations. We briefly discuss the implications of these observations for the design of microfluidic systems.

Keywords Lucas–Washburn · Capillary rise · Microfluidic channel

1 Introduction

The capillary-driven imbibition of liquids into tubes, channels and porous media is fundamental to a diverse range of applications, such as printing (Schoelkopf et al. 2002), lab-on-chip (Brody et al. 1996; Squires and Quake 2005), porous media (e.g., Marmur and Cohen 1997; Siebold et al. 2000) and soil water repellency (Shirtcliffe et al. 2006). The fundamental principles governing these types of problems are based on balancing the inertial forces, viscous forces, hydrostatic pressure and the capillary forces. Effective use and control of capillary imbibition

F. F. Ouali (✉) · H. Javed · M. I. Newton
School of Science and Technology, Nottingham Trent University, Clifton Lane, Nottingham NG11 8NS, UK
e-mail: fouzia.ouali@ntu.ac.uk

G. McHale · C. Trabi
Faculty of Engineering and Environment, Northumbria University, Ellison Place, Newcastle upon Tyne NE1 8ST, UK

N. J. Shirtcliffe
Faculty of Technology and Bionics, Rhine-Waal University of Applied Sciences, 47533 Kleve, Germany

requires an understanding of the different layers of subtlety that a problem may provide. Thus, there are different time regimes from the very early stage inertia dominated stage, described by Quéré (1997), to the late stage viscous regime of Lucas (1918) and Washburn (1921); the transition between these regimes for capillary rise is discussed by Fries and Dreyer (2008a). For horizontally mounted channels where gravity can be neglected and these regimes are described by the exact analytical Bousanquet solution (Bousanquet 1923), whose form is valid whether the channel is closed or open (e.g., Bouaidat et al. 2005; Jokinen and Franssila 2008); the Lucas–Washburn solution is the long time limit of the Bousanquet solution. We define a closed channel as one whereby all walls are solid and an open channel as one with a liquid–air interface as the effective wall. Due to its importance in microfluidics, capillary imbibition has previously been considered for a wide range of cross-sectional shape channels, such as circular (e.g., Stange et al. 2003), rectangular (e.g., Ichikawa et al. 2004; Jong et al. 2007; Zhu and Petkovic-Duran 2010) and grooved/triangular (Yost and Holm 1995; Romero and Yost 2006; Baret et al. 2007). Moreover, the same approach has been taken for channels defined by hydrophilic paths on a hydrophobic substrate (Darhuber et al. 2001) and by the space between two parallel plates (Rosendahl et al. 2004) under the assumption of flow with low Reynolds number and liquid imbibing in a tube/slab-like manner. When channels are mounted vertically gravity becomes important and exact analytical solutions for capillary imbibition are no longer possible in general. However, a visco-gravitational solution for time as a function of meniscus position does exist for the equivalent of the Lucas–Washburn regime (e.g., Krotov and Rusanov 1999; Hamraoui et al. 2000; Hamraoui and Nylander 2002), including for liquid–liquid systems (Mumley et al. 1986). In these problems, the role of the shape and wetting state of the walls are critical.

Advances in lithographic fabrication techniques are increasing the range of studies in which capillary aspects of imbibition and rise are critical. These advances are leading to studies with microfluidic (e.g., Yang et al. 2011) and nanofluidic capillaries widths of a few tens of nm (Han et al. 2006) or with depths as small as 6 nm (Oh et al. 2009). Whilst non-constant channel cross-sections have been a focus of study experimentally and theoretically (Legait 1983; Staples and Shaffer 2002; Reyssat et al. 2008; Liou et al. 2009), increased solid–liquid contact area, and hence increased capillary pull can be achieved using a range of in-channel structures. In a series of studies, Bico and co-workers studied imbibition using hemi-wicking, which amplifies the capillary pull using wall roughness (Bico 2000; Bico et al. 2002; Bico and Quéré 2003; Ishino et al. 2007); ideas recently applied to rough Cu_6Sn_5/Cu intermetallic surfaces (Liu et al. 2011). Their work used average parameters to characterize the capillary effect of roughness and topographic structures. This has been complemented by modeling studies by Kusumaatmaja et al. (2008) and Mognetti and Yeomans (2009) focused on feature shape and channel filling patterns, finite element modeling and experiments incorporating both capillary and viscous effects of flow through micropost (Srivastava et al. 2010; Byon and Kim 2011), and experimental studies using, e.g., stars, octagons and squares (Chen et al. 2009).

In hemi-wicking, the simplest viewpoint remains a capillary-driven penetration with a leading edge meniscus advancing in a tube/slab-like manner. However, the actual solid–liquid–vapor interface at the leading meniscus can be far more complicated as is known for capillary rise in square cross-section tubes, where the rise of a central meniscus is preceded by liquid fingers rising up the four internal edges. This reduces the equilibrium meniscus height by a factor of $(2 + \pi^{1/2})/4$ (Dong and Chatzis 1995; Bico and Quéré 2002). These effects are due to the wetting effects in corners and edges (Concus and Finn 1969; Ransohoff and Radke 1988; Ramé and Weislogel 2009; Girardo et al. 2009, 2012; Weislogel et al. 2011). Most recently, Ponomarenko et al. (2011) have studied the capillary rise of wetting liquids in the corners of different geometries and shown that in the viscous dominated regime the meniscus of these fingers rises without limit following a universal time$^{1/3}$ law, in contrast to the Lucas–Washburn time$^{1/2}$ law which eventually saturates at an equilibrium height. These geometry-induced wetting effects can be expected to affect both capillary rise and imbibition in microfluidic channels with non-circular cross-sections. There is therefore a need to study capillary-driven imbibition and rise within rectangular cross-section channels and with open and closed boundaries.

In this paper, we first provide in Sect. 2.1 an overview of the theoretical basis of capillary-driven rise and imbibition. We do so in a form that brings out the coherence of the equations and their solutions for different channel shapes in different orientations. We develop simple interpolation formulae for the viscous friction associated with open and closed rectangular channels of different aspect ratio. We show how within this formulation different contact angles on the various channel walls can be incorporated using surface free energy changes, including considerations of surface roughness or topography as required for hemi-wicking. Subsequently, in Sect. 2.2, we compare the exact numerical solution for capillary-driven imbibition to the various analytical solutions of the approximate equations with and without gravity. We obtain a condition for the cross-over time and rise height below which the Bousanquet solution is the best approximation and above which the visco-gravitational solution is a more accurate description. In Sect. 2.3, we discuss the sensitivity of imbibition for open rectangular channels to the value of

contact angle and the limitations of this approach when corner filling along edges between walls due to wetting is taken into account.

In Sects. 3 and 4 we present experiments on the capillary rise of polydimethylsiloxane (PDMS) oils in closed square tubes of glass and in open rectangular channels of SU-8. We observe that capillary rise in rectangular channels using PDMS oils involves a rising central meniscus, but with thin fingers spreading in advance of this main rise along the inside corner edges qualitatively consistent with the type of behavior described in Ponomarenko et al. (2011). The extent of advance of the fingers is sufficient to completely exit our channels. We find that fits to the numerical solution of the exact differential equation describing capillary rise, neglecting the fingers, up to the point where the fingers reach the ends of the channels can describe the rise of the central meniscus of the liquid in both of these cases. We also find that the friction in the open channel case is consistent with a non-rigidified liquid–air interface rather than for a rigidified boundary as recently reported for imbibition into horizontally mounted open microchannels (Yang et al. 2011).

2 Theoretical approach

2.1 Model formulation

In this section we review the standard analytical approach for describing capillary-driven imbibition in order to provide a common notation and clarity on the assumptions used, particularly with regards the wetting of the surfaces. Our aim is to consider the structure of the equations for uniform cross-section open and closed channels, but independent of precise geometry.

2.1.1 Momentum and gravity terms

We consider a tube (or "slab") of liquid of density ρ, constant cross-sectional area A_c and length $x(t)$ advancing along a channel displacing a gas phase. The rate of change of momentum is then,

$$\rho A_c \frac{d}{dt}\left(x\frac{dx}{dt}\right) = \rho A_c x \frac{d^2x}{dt^2} + \rho A_c \left(\frac{dx}{dt}\right)^2 \quad (1)$$

where t is time. The force driving the imbibition (or rise) is the capillary one and those resisting the imbibition are gravity and viscous forces. For a vertically mounted channel the gravitational force is,

$$f_{grav} = -\rho g \sin\varphi A_c x \quad (2)$$

where $g = 9.81\ \mathrm{m\ s^{-2}}$ is the acceleration due to gravity and φ is the angle of orientation of the channel to the horizontal.

2.1.2 Capillary terms

The capillary terms arise from the interchange or creation of solid–vapor, solid–liquid and liquid–vapor interfaces as the front of the tube of liquid advances. In this simplified model the profile of the solid–liquid–vapor interface is assumed to remain the same as a small advance forward, Δx, occurs. The surface free energy change ΔF as the liquid advances is then caused by changes in the various interfacial areas (Fig. 1),

$$\Delta F = \Delta x\left[\sum_i L_i^{SV\to SL}\left(\gamma_{SL}^i - \gamma_{SV}^i\right) + \sum_i L_i^{LV}\gamma_{LV}\right] \quad (3)$$

where the γ_{SL}^i and γ_{SV}^i are the interfacial energies per unit area relating to the ith solid wall element, γ_{LV} is the surface tension of the liquid, $L_i^{SV\to SL}$ is the perimeter length of the ith solid wall element on which contact with vapor is replaced by contact with the liquid, and L_i^{LV} is the perimeter length of any liquid–vapor interface created. Since the Young's law contact angle is $\cos\theta_e^i = (\gamma_{SV}^i - \gamma_{SL}^i)/\gamma_{SV}^i$ and the capillary force, f_{cap}, is $(-\Delta F/\Delta x)$ in the limit of $\Delta x \to 0$, we obtain,

$$f_{cap} = \gamma_{LV}\left[\sum_i L_i^{SV\to SL}\cos\theta_e^i + \sum_i L_i^{LV}\cos\left(180^\circ\right)\right] \quad (4)$$

where $\cos(180°) = -1$ has been used to show the similarity in the terms when the interface between a liquid and vapor is regarded as a perfectly hydrophobic surface.

Figure 2 shows three specific channel geometries: (a) circular cross-section tube of radius R, (b) closed and (c) open rectangular channel of width W and depth H. In each case, it is assumed that the solid surfaces can have different surface chemistries (i.e., contact angles). In the simplest case of a tube, only the first term contributes and the perimeter length is $2\pi R$ so that Eq. (4) becomes,

$$f_{cap}^{tube} = 2\pi R\gamma_{LV}\cos\theta_e \quad (5)$$

In the case of the closed and open rectangular channels, Eq. (4) becomes,

$$f_{cap}^{rect} = \gamma_{LV}W\left[\cos\theta_e^B + \cos\theta_e^T + \varepsilon\left(\cos\theta_e^L + \cos\theta_e^R\right)\right] \quad (6)$$

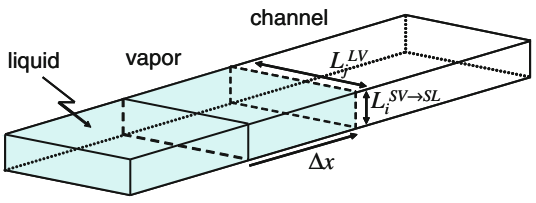

Fig. 1 Surface free energy changes as a tube/slab of liquid penetrates into a channel resulting in new solid–liquid and liquid–vapor interfaces

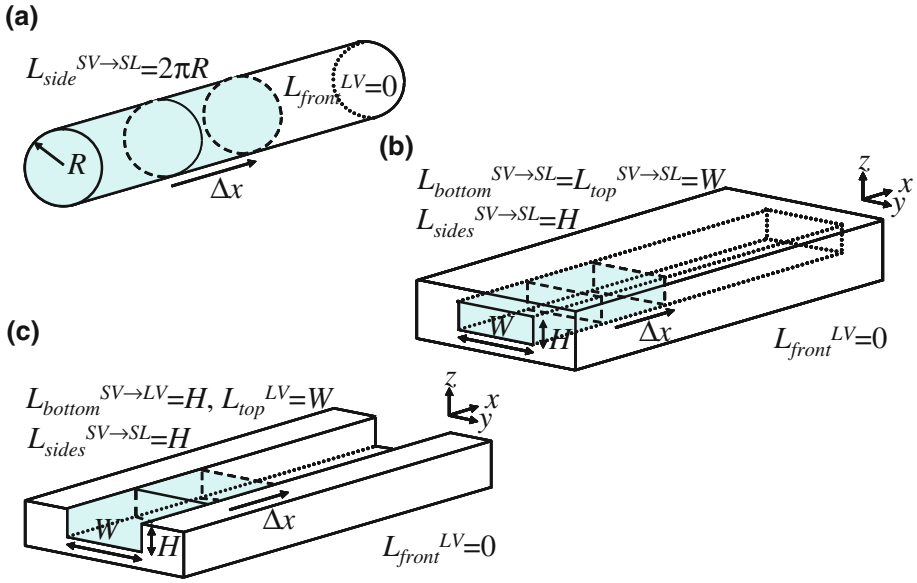

Fig. 2 Solid–liquid and liquid–vapor interfaces associated with, **a** circular cross-section tube, **b** closed rectangular channel, and **c** open rectangular channel

where $\varepsilon = H/W$ and (B, T, L, R) label the contact angles for the bottom, top and left and right hand side surfaces; for the open channel $\theta_e^{\mathrm{T}} = 180°$ is used in Eq. (6).

Other shaped channels, such as a tube of elliptical cross-section and V-shaped grooves or triangular channels, can be assessed in the same manner from Eq. (4). For example, an open or closed V-shaped channel of width W and depth H gives,

$$f_{\mathrm{cap}}^{\mathrm{groove}} = \gamma_{\mathrm{LV}} W \left[\cos\theta_e^{\mathrm{T}} + \frac{1}{2}\sqrt{1+4\varepsilon^2}\left(\cos\theta_{\mathrm{e}}^{\mathrm{L}} + \cos\theta_{\mathrm{e}}^{\mathrm{R}}\right) \right] \tag{7}$$

where $\theta_{\mathrm{e}}^{T} = 180^{\circ}$ gives the open groove result. For the case of flow between two parallel plates with open sides along a path defined by a hydrophilic stripe on the plates, Eq. (6) with $\theta_{\mathrm{e}}^{\mathrm{L}} = 180^{\circ}$ and $\theta_{\mathrm{e}}^{\mathrm{R}} = 180^{\circ}$ can be used.

2.1.3 Capillary terms and surface roughness

A slightly more complex situation is when one or more of the surfaces are rough or topographically structured at the small scale. In the Wenzel case the liquid fully penetrates into the surface features whereas in the Cassie-Baxter state the liquid bridges between surface features (Quéré 2008; Shirtcliffe et al. 2010). When the contact angle is well below 90°, surface roughness can drive enhanced spreading (e.g., McHale et al. 2004). Using the surface free energy argument, Eq. (4) becomes,

$$f_{\mathrm{cap}} = \gamma_{\mathrm{LV}} \left[\sum_i L_i^{\mathrm{SV}\to\mathrm{SL}} \cos\theta_{\mathrm{T}}^i + \sum_i L_i^{\mathrm{LV}} \cos\left(180^{\circ}\right) \right] \tag{8}$$

where the Young's law contact angle, θ_{e}^i, is replaced by the Wenzel or Cassie-Baxter contact angle, θ_{T}^i with $\theta_{\mathrm{T}}^i = \theta_{\mathrm{W}}^i$ or $\theta_{\mathrm{T}}^i = \theta_{\mathrm{CB}}^i$, and $L_i^{\mathrm{SV}\to\mathrm{SL}}$ is the planar projection of the perimeter length of the ith solid wall element across which the liquid advances. The Wenzel and Cassie-Baxter contact angles are defined by,

$$\cos\theta_{\mathrm{W}} = r_{\mathrm{s}} \cos\theta_{\mathrm{e}} \tag{9}$$

and

$$\cos\theta_{\mathrm{CB}} = \varphi_{\mathrm{s}} \cos\theta_{\mathrm{e}} - (1 - \varphi_{\mathrm{s}}) \tag{10}$$

where r_{s} is the roughness at the contact line and φ_{s} is the solid surface fraction. More generally, a mixed partially penetrating state may exist and θ_{T}^i then takes on the appropriate value taking into account both surface roughness and solid surface fraction (Shirtcliffe et al. 2010). Thus, Eqs. (5)–(7) attempt to take into account the effect of roughness or topography on the capillary drive for imbibition simply by the replacement of the contact angle by the appropriate Wenzel, Cassie-Baxter or mixed state one involving both the surface chemistry and surface structure. This approach based on minimizing surface free energy changes does not take into account contact line pinning and hysteresis.

2.1.4 Viscous terms and interpolation formulae

The viscous force for flow down a tube or a channel can be deduced from the flow velocity profile assuming incompressible, Newtonian liquid with a laminar flow, and solving the continuity and Navier–Stokes equations. For the closed rectangular channel geometry, Brody et al. (1996) give the general approach and solution for the flow (see also Ichikawa et al. 2004). The non-zero component of the equations relates the flow velocity, $u(y, z)$, in the x-direction to the pressure gradient,

$$\frac{\partial^2 u}{\partial y^2}+\frac{\partial^2 u}{\partial z^2}=\frac{1}{\eta}\left(\frac{\mathrm{d}p}{\mathrm{d}x}\right) \tag{11}$$

where η is the viscosity and $p(x)$ is the pressure profile which only depends upon x. This equation can be solved for a channel of arbitrary aspect ratio $\varepsilon = H/W$ using a Fourier series approach to obtain a general solution for $u(y, z)$ to which non-slip boundary conditions can then be applied for the upper and lower channel surfaces. To work out the viscous force we first evaluate the depth and width averaged value of the flow velocity of the closed channel, $u^{\mathrm{c}}_{\mathrm{ave}}$,

$$u^{\mathrm{c}}_{\mathrm{ave}}=\left(-\frac{\mathrm{d}p}{\mathrm{d}z}\right)\left(\frac{8H^2}{\eta\pi^4}\right)\sum_{l=0}^{\infty}\frac{1}{(2l+1)^4} \times\left[1-\left(\frac{2\varepsilon}{(2l+1)\pi}\right)\tanh\left(\frac{(2l+1)\pi}{2\varepsilon}\right)\right] \tag{12}$$

This allows us to write the pressure gradient in terms of the average flow velocity so that the flow profile is,

$$u(y,z)=\left(\frac{48u^{\mathrm{c}}_{\mathrm{ave}}}{\pi^3\zeta_{\mathrm{c}}(\varepsilon)}\right)\sum_{l=0}^{\infty}\frac{(-1)^l}{(2l+1)^3} \times\left[1-\frac{\cosh\left(\alpha^{\mathrm{c}}_l y/W\right)}{\cosh\left(\alpha^{\mathrm{c}}_l/2\right)}\right]\cos\left(\alpha^{\mathrm{c}}_l z/W\right) \tag{13}$$

where $\alpha^{\mathrm{c}}_l=\frac{(2l+1)\pi}{\varepsilon}$ and we have defined an aspect ratio function, $\zeta_{\mathrm{c}}(\varepsilon)$, as

$$\zeta_c(\varepsilon)=\left(\frac{96}{\pi^4}\right)\sum_{l=0}^{\infty}\frac{1}{(2l+1)^4}\left[1-\frac{2\tanh\left(\alpha^{\mathrm{c}}_l/2\right)}{\alpha^{\mathrm{c}}_l}\right] \tag{14}$$

The viscous force on the top, bottom and two walls of the rectangular channel is then,

$$f^{\mathrm{c}}_{\mathrm{visc}}=2x\eta\left[\int_{-W/2}^{W/2}\left(\frac{\partial u(y,z)}{\partial z}\right)_{z=H/2}\mathrm{d}y+\int_{-H/2}^{H/2}\left(\frac{\partial u(y,z)}{\partial y}\right)_{y=W/2}\mathrm{d}z\right] \tag{15}$$

which gives,

$$f^{\mathrm{c}}_{\mathrm{visc}}=-\frac{12\eta x u^{\mathrm{c}}_{\mathrm{ave}}}{\varepsilon\zeta_{\mathrm{c}}(\varepsilon)} \tag{16}$$

This form makes obvious the relationship between flow in a closed rectangular channel of arbitrary aspect ratio and the one-dimensional result because in the limit of a shallow and infinitely wide channel, i.e., $W \to \infty$, the aspect ratio function $\zeta_{\mathrm{c}}(\varepsilon) \to 1$.

Repeating the previous approach for an open channel gives,

$$u^{\mathrm{o}}_{\mathrm{ave}}=\left(\frac{8GW^2}{\eta\pi^4}\right)\sum_{l=0}^{\infty}\frac{1}{(2l+1)^4}\left[\frac{\tanh((2l+1)\pi\varepsilon)}{(2l+1)\pi\varepsilon}-1\right] \tag{17}$$

which allows the pressure gradient to be written in terms of the average flow velocity so that the flow profile is,

$$u(y,z)=-\left(\frac{12u^{\mathrm{o}}_{\mathrm{ave}}}{\pi^3\varepsilon^2\zeta_{\mathrm{o}}(\varepsilon)}\right)\sum_{l=0}^{\infty}\frac{(-1)^l}{(2l+1)^3} \times\left[\cosh\left(\alpha^{\mathrm{o}}_l z/H\right)-\tanh\alpha^{\mathrm{o}}_l\sinh\left(\alpha^{\mathrm{o}}_l z/H\right)-1\right]\cos\left(\alpha^{\mathrm{o}}_l y/H\right) \tag{18}$$

where $\alpha^{\mathrm{o}}_l=(2l+1)\pi\varepsilon$ and we have defined an aspect ratio function, $\zeta_{\mathrm{o}}(\varepsilon)$, as

$$\zeta_{\mathrm{o}}(\varepsilon)=\left(\frac{24}{\pi^4\varepsilon^2}\right)\sum_{l=0}^{\infty}\frac{1}{(2l+1)^4}\left[1-\frac{\tanh\alpha^{\mathrm{o}}_l}{\alpha^{\mathrm{o}}_l}\right] \tag{19}$$

The viscous force on the bottom (but not top) and two walls of the rectangular channel is then,

$$f^{\mathrm{o}}_{\mathrm{visc}}=-\eta\left[\int_{-W/2}^{W/2}\left(\frac{\partial u(y,z)}{\partial z}\right)_{z=0}\mathrm{d}y+2\int_{0}^{H}\left(\frac{\partial u(y,z)}{\partial y}\right)_{y=W/2}\mathrm{d}z\right] \tag{20}$$

which gives,

$$f^{\mathrm{o}}_{\mathrm{visc}}=-\frac{3\eta x u^{\mathrm{o}}_{\mathrm{ave}}}{\varepsilon\zeta_{\mathrm{o}}(\varepsilon)} \tag{21}$$

In a similar manner to the closed rectangular channel result, Eq. (16), this form makes obvious the relationship between flow in an open rectangular channel of arbitrary aspect ratio and the one-dimensional result because in the limit of a shallow and infinitely wide channel, i.e., $W \to \infty$, the aspect ratio function $\zeta_{\mathrm{o}}(\varepsilon) \to 1$. It should be noted that alternative, but equivalent Fourier series solutions for the flow in an open rectangular exist, such as that in Baret et al. (2007) and Yang et al. (2011).

Whilst Eq. (14) and Eq. (19) are exact, it is useful for fitting to experimental data to have simple interpolation formulae. For channels with aspect ratios in the range $\varepsilon = 0.0$–2.0, we find suitable interpolations with limits of unity as $\varepsilon \to 0$ are given by,

$$\zeta^{-1}_{\mathrm{c}}(\varepsilon)\approx 1+0.362374\varepsilon+1.020980\varepsilon^2 \tag{22}$$

and

$$\zeta^{-1}_{\mathrm{o}}(\varepsilon)\approx 1+0.671004\varepsilon+4.169711\varepsilon^2 \tag{23}$$

Figure 3 shows the exact summations given by Eq. (14) and Eq. (19) and the interpolations from Eq. (22) and Eq. (23). Below aspect ratios of 0.60, the agreement is good to around 3 % or better and above this aspect ratio up to $\varepsilon = 2.0$ is better

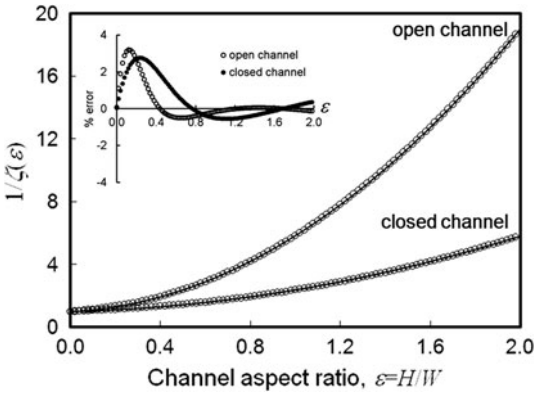

Fig. 3 Geometric factors in the viscous force for flow in *open* and *closed rectangular* channels with aspect ratio $\varepsilon = H/W$ between 0 and 2.0. The *symbols* are the exact results and the *solid lines* are the interpolation formulae. The *inset* shows the corresponding % error between the two

than 1 % (as shown in the inset of Fig. 3). A similar approach could also be adopted for flow in other shapes of channels, such as triangular grooves (Ayyaswamy et al. 1974).

For completeness, we note the standard expression for viscous force for flow in a circular cross-section tube,

$$f_{\text{visc}}^{\text{tube}} = -8\eta\pi x u_{\text{ave}}^{\text{tube}} \tag{24}$$

2.1.5 Defining equation and its assumptions

The equation describing capillary-driven imbibition is given by combining Eqs. (1), (2) and (8) with Eqs. (16), (21) or (24) as appropriate for the channel or tube and assuming $u_{\text{ave}} = \mathrm{d}x/\mathrm{d}t$ can be used,

$$\frac{1}{2}\frac{\mathrm{d}}{\mathrm{d}t}\left(\frac{\mathrm{d}x^2}{\mathrm{d}t}\right) = b - g\sin\varphi\, x - ax\left(\frac{\mathrm{d}x}{\mathrm{d}t}\right) \tag{25}$$

In this equation, the viscous coefficient a has dimensions of inverse time (s^{-1}) and is defined for the tube, closed rectangular channel and open rectangular channel as,

$$a = \begin{cases} 8\eta/\rho R^2 \\ 12\eta/\rho H^2\zeta_{\text{c}}(\varepsilon) \\ 3\eta/\rho H^2\zeta_{\text{o}}(\varepsilon) \end{cases} \tag{26}$$

and the capillary coefficient term b has dimensions of speed^2 ($\mathrm{m}^2\ \mathrm{s}^{-2}$) and is defined in these three cases as,

$$b = \frac{\gamma_{\text{LV}}}{\rho A_{\text{c}}}\left[\sum_i L_i^{\text{SV}\to\text{SL}}\cos\theta_{\text{T}}^i - \sum_i L_i^{\text{LV}}\right] = \begin{cases} 2\gamma_{\text{LV}}\cos\theta_{\text{e}}/\rho R \\ \gamma_{\text{LV}}\left[\cos\theta_{\text{e}}^{\text{B}} + \cos\theta_{\text{e}}^{\text{T}} + \varepsilon\left(\cos\theta_{\text{e}}^{\text{L}} + \cos\theta_{\text{e}}^{\text{R}}\right)\right]/\rho H \\ \gamma_{\text{LV}}\left[\cos\theta_{\text{e}}^{\text{B}} + \cos\theta_{\text{e}}^{\text{T}} + \varepsilon\left(\cos\theta_{\text{e}}^{\text{L}} + \cos\theta_{\text{e}}^{\text{R}}\right)\right]/\rho H \end{cases} \tag{27}$$

For closed channels with smooth surfaces and the same contact angle on all surfaces θ_{e}, $b = 2\gamma_{\text{LV}}\cos\theta_{\text{e}}(1+\varepsilon)/\rho H$. For open rectangular channels, the free surface vapor boundary acts as a perfect hydrophobic surface (i.e., $\theta_{\text{e}}^{\text{T}} = 180^{\circ}$), and if all other contact angles are the same, $b = \gamma_{\text{LV}}[\cos\theta_{\text{e}}(1+2\varepsilon) - 1]/\rho H$. The capillary coefficient b [Eq. (27)] can thus be written for the three cases as:

$$b = \begin{cases} 2\gamma_{\text{LV}}\cos\theta_{\text{e}}/\rho R \\ 2\gamma_{\text{LV}}\cos\theta_{\text{e}}(1+\varepsilon)/\rho H \\ \gamma_{\text{LV}}[\cos\theta_{\text{e}}(1+2\varepsilon) - 1]/\rho H \end{cases} \tag{28}$$

Equation (25) is well known in the theory of capillary-driven imbibition, but is written here in a form that emphasizes the similarities between circular cross-section tubes, closed and open rectangular channels of arbitrary aspect ratio. Moreover, it allows the key assumptions to be easily identified and their influence on the structure of Eq. (25) to be assessed. For example, using the open form for viscous dissipation in an open rectangular channel assumes that momentum can be transferred across the liquid–vapor interface as liquid flows up the tube of liquid to extend itself. However, as indicated by Yang et al. (2011) in their study on the capillary flow in horizontally oriented shallow open rectangular channels ($H = 19$ μm and $W = 15$, 25, 50 and 75 μm) a rigidified liquid–vapor interface can occur due to contaminants or surfactants on the liquid–vapor interface. Their fitting therefore used the viscous parameter a from Eq. (26) for a closed rectangular channel with the capillary b parameter from Eq. (27) for an open rectangular channel.

The assumptions in the approach in Sects. 2.1.2 and 2.1.3 taken to derive the capillary terms is that they include a quasi-equilibrium advancing state and this leads to the Young's law equilibrium contact angle, θ_{e}. Many authors have questioned this and replaced the contact angle by either the advancing contact angle or the velocity-dependent dynamic contact angle Hoffman's formula (Siebold et al. 2000; Chebbi 2007) or molecular-kinetic theory (Hamraoui et al. 2000; Hamraoui and Nylander 2002; Blake and Coninck 2004) or have considered a range of possible dynamic contact angle relationships (e.g., Popescu et al. 2008). It is also possible that a quasi-equilibrium meniscus shape may be achieved, but only after an initial capillary penetration. Even after the initial penetration, a further assumption is that the profile of the liquid meniscus advances in a tube/slab-like manner without change and this we examine further in Sect. 2.3 using wetting concepts commonly used for corner filling problems. Possibly one of the most limiting aspects in complex shape channels is that a given wetting state, such as a Cassie-Baxter, Wenzel or mixed state arising from minimum surface free energy change considerations, is not known a priori. Moreover, the extent of hysteresis and asymmetric imbibition properties can be linked to complex topographies (e.g., Kusumaatmaja et al. 2008). Thus for capillary filling in channels of complex shapes alternatives to a purely analytical (with numerical solution) approach that have

been considered include the Lattice Boltzmann approach (e.g., Kusumaatmaja et al. 2008; Clime et al. 2012), numerical simulation using diffuse interface models (e.g., Mehrabian et al. 2011), smoothed particle hydrodynamics (e.g., Tartakovsky and Meakin 2005) and molecular-dynamics (e.g., Ahadian et al. 2009; Stukan et al. 2010).

2.2 Exact and approximate solutions

Equation (25) predicts that experiments on capillary-driven imbibition/rise into channels of different cross-sectional shapes and with open and closed surfaces will show the same type of behavior, but each will have its own length and timescales determined by the appropriate form of the two parameters a and b. Whilst it cannot be solved exactly, approximate solutions can be obtained for the different characteristic length and time scales. Fries and Dreyer (2009) discuss a systematic approach to obtaining dimensionless scaling for the case of a cylindrical tube and porous media using the Buckingham π theorem.

2.2.1 *Bousanquet solution for a horizontal capillary*

To obtain a dimensionless form of Eq. (25) we scale the position and time coordinates as $T = at$ and $X = ax/(2b)^{1/2}$,

$$\left(\frac{\mathrm{d}^2X^2}{\mathrm{d}T^2}\right) = 1 - G\sin\varphi X - \left(\frac{\mathrm{d}X^2}{\mathrm{d}T}\right) \tag{29}$$

where we have defined a dimensionless constant $G = g(2/b)^{1/2}/a$. Using Eq. (26) and Eq. (28) the tube, closed and open channel cases are,

$$G = \begin{cases} \sqrt{\dfrac{g^2\rho^3R^5}{64\eta^2\gamma_{\mathrm{LV}}\cos\theta_{\mathrm{e}}}} \\ \sqrt{\dfrac{g^2\rho^3H^5\zeta_{\mathrm{c}}^2(\varepsilon)}{144\eta^2(1+\varepsilon)\gamma_{\mathrm{LV}}\cos\theta_{\mathrm{e}}}} \\ \sqrt{\dfrac{2g^2\rho^3H^5\zeta_{\mathrm{o}}^2(\varepsilon)}{9\eta^2\gamma_{\mathrm{LV}}[(1+2\varepsilon)\cos\theta_{\mathrm{e}}-1]}} \end{cases} \tag{30}$$

The dimensionless form given in Eq. (29) corresponds to the Fries and Dreyer (2009) case 3 where the basic parameter is gravity and the scaling parameters are inertia and viscosity. Our definitions of X and T are not identical to their scaled variables in the case of a tube, but our controlling parameter G is simply related to their Ω by $G = 2^{1/2}/\Omega$. When $G\sin\varphi \to 0$ so that the capillary is horizontally oriented, the solution to Eq. (29) is the Bousanquet solution (1923),

$$X^2(T) = T - [1 - \exp(-T)] \tag{31}$$

At long timescales when $T \gg 1$ (i.e., $t \gg 1/a$), Eq. (31) gives $X(T) \approx T^{1/2}$ or $x(t) = (2b/a)^{1/2}t^{1/2}$, which is the Lucas–Washburn solution when the viscous term dominates; effectively the first term in Eq. (29) can be ignored. At short timescales when $T \ll 1$ (i.e., $t \ll 1/a$), Eq. (31) gives $X(T) \approx T/\sqrt{2}$ or $x(t) = b^{1/2}t$, which is the inertial solution of Quéré (1997) with a linear imbibition with time; effectively the last term in Eq. (29) can be ignored.

In fitting experimental data for imbibition into horizontal channels, the full Bousanquet solution [Eq. (31)] can be used provided data is captured across both the long and short timescales as determined by $1/a$. If data for only short or only long timescales is captured then either the Quéré (Inertial) or Lucas–Washburn (Viscous) solutions should be used.

2.2.2 *Viscous solution for a vertical capillary*

When $T \gg 1$ and the inertial term can be ignored, but gravity cannot be neglected, Eq. (29) becomes,

$$0 = 1 - G\sin\varphi X - \left(\frac{\mathrm{d}X^2}{\mathrm{d}T}\right) \tag{32}$$

As shown by Washburn (1921), and discussed by Fries and Dreyer (2008b) (see also Mumley et al. 1986; Krotov and Rusanov 1999), this has an analytical solution, but for time as function of position rather than for position as a function of time. By rearranging Eq. (32) to,

$$\frac{2X}{1 - G\sin\varphi X}\left(\frac{\mathrm{d}X}{\mathrm{d}T}\right) = 1 \tag{33}$$

an exact integration can be performed to get the visco-gravitational solution,

$$T = \frac{-2}{(G\sin\varphi)^2}[G\sin\varphi X + \log(1 - G\sin\varphi X)] \tag{34}$$

where $X = 0$ at $T = 0$ has been assumed. When $G\sin\varphi X \to 0$, the $\log(1 - G\sin\varphi X)$ can be expanded and this gives $T \approx X^2$, which is the Lucas–Washburn solution. As $G\sin\varphi X \to 1$, the logarithm diverges so that $T \to \infty$ and so at equilibrium the capillary rise height is $X_{\mathrm{e}} = 1/(G\sin\varphi)$, i.e., $x_{\mathrm{e}} = b/(g\sin\varphi)$. Fries and Dreyer (2008b) discuss the problems of inverting Eq. (34) and also provide an analytic solution in terms of the Lambert $W(x)$ function defined by $w = W(w)\exp(W(x))$. Equation (34) can be rewritten in terms of x and t as

$$t = -\frac{ab}{(g\sin\varphi)^2}\left(\frac{x}{x_{\mathrm{e}}} + \ln\left(1 - \frac{x}{x_{\mathrm{e}}}\right)\right) \tag{35}$$

In fitting experimental data for imbibition into vertical channels ($\varphi = 90°$) the viscous-gravitational solution [Eq. (34) or Eq. (35)] can be used provided data is captured including both the early Lucas–Washburn stage $T \approx X^2$ and the approach to equilibrium as determined by $x \to b/g$. The fact Eq. (35) is an analytical solution with

time as a function of position, which cannot be easily inverted, does not prevent fitting of experimental data since time can be fitted as a function of measured position as easily as position as a function of measured time.

2.2.3 Inertial solution for a vertical capillary

When $T \gg 1$ and the viscous term can be ignored, but gravity cannot be neglected, Eq. (29) becomes,

$$\left(\frac{\mathrm{d}^2X^2}{\mathrm{d}T^2}\right) = 1 - G\sin\varphi X \tag{36}$$

There is no obvious closed form solution to Eq. (36), but a perturbation solution can be constructed for X as a power series in G sin φ (Quéré 1997). When G sin $\varphi = 0$ the zeroth order solution is $X_o^2(T) = T^2/2$. We then write $X(T) \approx X_o + G$ sin $\varphi\, X_1$ and substitute into Eq. (36) and keep first order terms in G sin φ,

$$\left(\frac{\mathrm{d}^2(TX_1)}{\mathrm{d}T^2}\right) \approx -\frac{T}{2} \tag{37}$$

This has a solution $X_1(T) = -T^2/12$, which gives a gravity modified inertial solution of,

$$X(T) \approx \frac{T}{\sqrt{2}}\left(1 - \frac{\sqrt{2}G\sin\varphi\, T}{12}\right) \tag{38}$$

or in non-scaled quantities,

$$x(t) \approx \sqrt{b}t\left(1 - \frac{g\sin\varphi\, t}{6\sqrt{b}}\right) \tag{39}$$

Equation (38) can also be inverted to give,

$$T(X) \approx \sqrt{2}X\left(1 + \frac{G\sin\varphi X}{6}\right) \tag{40}$$

2.2.4 Cross-over between Bousanquet and visco-gravitational solutions

Equation (29) can be solved numerically for any value of G sin φ using the inertial approximation for the initial boundary conditions $X(0) = 0$ and $(\mathrm{d}X^2/\mathrm{d}T)_{T=0} = 0$. Figure 4 shows the behavior of $X(T)$ as a fraction of the equilibrium height, X_e, for $G = 0.1$ and $\varphi = 90°$ together with the, Bousanquet, Lucas–Washburn and inertial approximations. Perhaps surprisingly even at capillary rise heights up to 20 % of the equilibrium height both the Lucas–Washburn and the viscous-gravitational approximations show substantial differences from the exact solution. Moreover, this is not significantly improved using the first order gravitational correction to the inertial approximation. Numerically the initial rise height is best described by the Bousanquet solution [Eq. (31)] until it crosses over with the visco-gravitational solution [Eq. (34)] at around

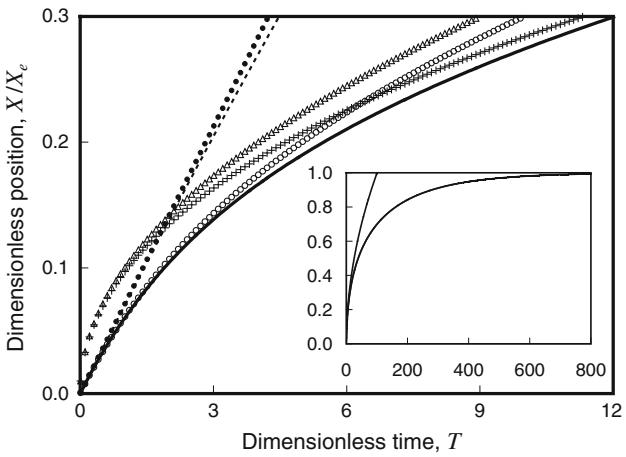

Fig. 4 Comparison of approximate analytical solutions for Bousanquet (*open circle*), visco-gravitational (*plus symbol*), Lucas–Washburn (*open triangle*), inertial (*filled circle*) and inertial with gravity correction (*dashed line*) to the exact numerical solution (*solid line*) for $G = 0.1$ and $\varphi = 90°$. The capillary rise height X is shown as a fraction of the equilibrium rise height, X_e. The *inset* shows the long time behavior for the exact solution and the Bousanquet solution. On this scale the visco-inertial cannot be distinguished from the exact solution and the Lucas–Washburn approximation cannot be distinguished from the Bousanquet solution on the longer time scale

$(T, X/X_e) = (6.5, 0.22)$. Above this cross-over the visco-gravitational solution ever more closely agrees with the exact numerical solution as the rise height tends to its equilibrium value; however, it always lies above the exact numerical solution. Since the curve exponentially approaches equilibrium as $(X - X_e)/X_e \sim \exp(-G^2T/2)$, fitting experimental data taken in the long time limit using Eq. (34) could force better agreement by overestimating G.

The derivative $\mathrm{d}X/\mathrm{d}T$ can be calculated for each of Eq. (31) and Eq. (34) and this shows that in the Bousanquet case the initial slope of $X(T)$ is $1/\sqrt{2}$ whereas in the visco-gravitational case the initial slope tends to infinity as $1/2X$. Since in both cases the slopes are positive at all positive T and in the visco-gravitational case $X \to X_e = 1/(G$ sin $\varphi)$ whereas in the Bousanquet case $X \to \infty$, there is one and only one cross-over point (T_c, X_c) at which the two curves meet. The cross-over time, T_c, can be calculated numerically as a function of G sin φ by equating the Bousanquet solution [Eq. (31)] to the visco-gravitational solution [Eq. (34)]. For a vertical channel with $\varphi = 90°$ this is shown in Fig. 5 (open circles symbols and left hand y-axis) as a function of $G = 1/X_e$. A numerical interpolation of this function accurate to 3.7 % in T_c over the range $G = 1 \times 10^{-7}$ to 1.0 is given by a two-thirds power law,

$$T_c(G) \approx \frac{1.341}{G^{2/3}} = 1.341X_e^{2/3} \tag{41}$$

The validity of the two-thirds power law can be shown analytically for small G although the pre-factor in Eq. (41)

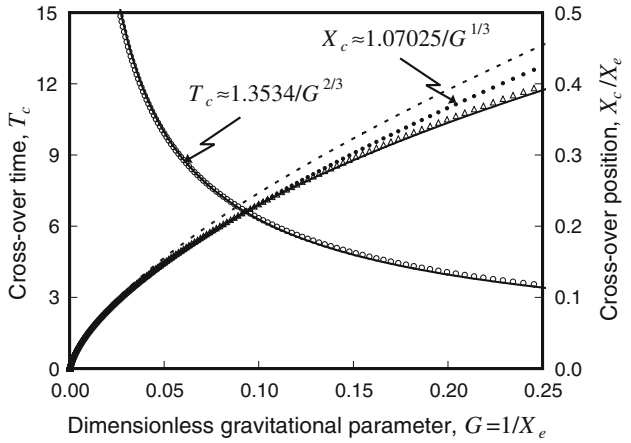

Fig. 5 Cross-over time, T_c, at which the visco-inertial solution better approximates the exact numerical solution than the Bousanquet solution (*circle symbol* and left hand *y*-axis); the *solid line* is the interpolation $T_c \approx 1.3534X_e^{2/3}$ optimized for G up to 0.25 with $\varphi = 90°$ (left hand *y*-axis). Capillary rise height X_c/X_e at the cross-over calculated numerically (*triangle symbol*) and an interpolation using $X_c \approx 1.07025/G^{1/3}$ (*dotted line*). Using the interpolation of T_c in the Bousanquet equation gives an improved estimate of X_c (*solid line* through *triangle symbols*); the *dashed line* shows the analytical approximation $X_c \approx (3/2)^{1/3}X_e^{1/3}$

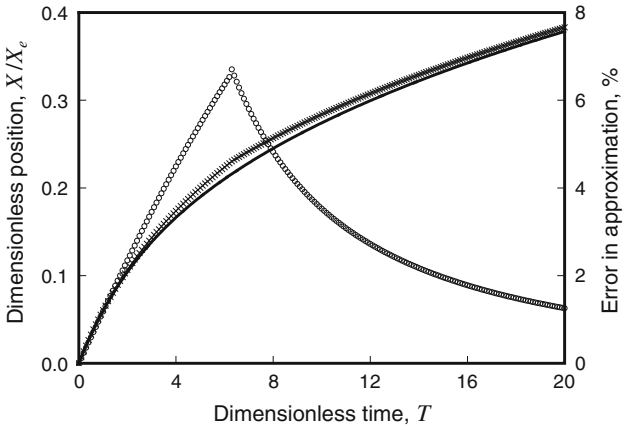

Fig. 6 The exact solution for $G = 0.1$ and $\varphi = 90°$ (*solid curve* and left hand *y*-axis) and the approximation obtained using the lower value for X taken from the Bousanquet and the visco-gravitational solutions (*crosses* and left hand *y*-axis). The percentage error using the approximation peaks at T_c (*circles* and right hand *y*-axis)

is found to be $(3/2)^{2/3} = 1.3104$. Numerically, using 1.3104 is accurate to 4 % in the range of G up to 0.1, to 1 % in the range of G up to 0.01, and 5.8 % in the range of G up to up to 1.32. A best fit interpolation for the numerically calculated rise height at which the cross-over, X_c, occurs over the range up to $G = 0.25$ is given by $1.07025/G^{1/3}$; the exact numerical calculation is shown in Fig. 5 by the open triangles symbols (right hand *y*-axis) and the interpolation is the dotted line. An improved estimate is given by using the interpolation for T_c in the Bousanquet solution [Eq. (31)] and this is shown as the solid line passing through the open triangles symbols.

To derive the two-thirds power law for T_c we expand the log term in the visco-gravitational approximation [Eq. (34)] to 3rd order and regroup terms to get,

$$\frac{X^2}{(T-X^2)^{2/3}} \approx \left(\frac{3}{2G\sin\varphi}\right)^{2/3} \tag{42}$$

From the Bousanquet solution [Eq. (31)], we then note that,

$$\frac{X^2}{(T-X^2)^{2/3}} = T_c\left[\frac{1-(1-e^{-T})/T}{(1-e^{-T})^{2/3}}\right] = Tf(T) \tag{43}$$

which defines a function $f(T)$. Combining Eq. (42) and Eq. (43) at $(T, X) = (T_c, X_c)$ then gives,

$$T_c f(T_c) \approx \left(\frac{3}{2G\sin\varphi}\right)^{2/3} = \left(\frac{3X_e}{2}\right)^{2/3} \tag{44}$$

when the cross-over time is large $f(T_c) \to 1$ and when it is small $f(T_c) \to 0.5T_c^{1/3}$ so that the power law changes from two-third to half as T_c becomes small. Since large T_c corresponds to small G sin φ (i.e., large X_e) we obtain the numerically observed two-third power law with the pre-factor of $(3/2)^{2/3} = 1.3104$. This also suggests that the fractional cross-over rise height for small G sin φ will be,

$$\frac{X_c}{X_e} \approx \left(\frac{3}{2X_e^2}\right)^{1/3} = \frac{1.1447}{X_e^{2/3}} \tag{45}$$

and this is shown in Fig. 5 as the dashed line (referenced to the right hand side y-axis).

The Bousanquet and visco-gravitational solutions can be combined to provide an overall approximate solution by using the former solution when $T < T_c$ and the latter solution when $T > T_c$ [i.e., the solution predicting the lower capillary rise $X(T)$]. This provides a broad time range approximate solution as shown in Fig. 6 for $G = 0.1$. Figure 6 also illustrates the percentage error between the exact solution and this approximate solution for a vertical capillary with $\varphi = 90°$, which has a maximum error of 6.7 % at $T = 6.3$ when $X_c/X_e = 0.216$. For $G = 0.0283$, corresponding to a cross-over at $X_c/X_e = 0.1$, the maximum error is 3.2 % and for $G = 0.814$, corresponding to a cross-over at $X_c/X_e = 0.7$, maximum error is around 17 %.

2.3 Filling conditions and capillary fingers

According to the approach in Sect. 2.2, for capillary-driven imbibition to commence it has to be energetically favourable for the liquid to enter the channel, i.e., the surface free energy change in Eq. (3) must satisfy $\Delta F < 0$, or equivalently the capillary force in Eq. (4) must satisfy $f_c > 0$ and the b parameter in Eq. (27) must be positive. Thus, for an open or closed rectangular channel,

$$\cos\theta_e^B + \cos\theta_e^T + \varepsilon\left(\cos\theta_e^L + \cos\theta_e^R\right) > 0 \quad (46)$$

For a closed channel with smooth surfaces and the same contact angle on all surfaces this simply means the contact angle must be less than 90°. However, for an open rectangular channel $\theta_e^T = 180°$ and so the condition becomes,

$$\cos\theta_e > \frac{1}{1+2\varepsilon} \quad (47)$$

as noted by previous authors. Therefore, as the aspect ratio of a rectangular channel reduces imbibition becomes increasingly difficult and lower contact angles corresponding to more wetting liquids are required. For example, aspect ratios of $\varepsilon = 10$, 0.6, 0.3 and 0.2 require contact angles below 78.5°, 63.0°, 51.3° and 44.4°. Effectively the capillary pull required is principally from the wall area which becomes relatively less as the width of channel increases.

From an experimental perspective the accuracy of quantitative estimates of the capillary coefficient b parameter in both the inertial (Quéré) and viscous (Lucas–Washburn) regimes from the initial imbibition data become more difficult for open rectangular channels. In these cases data is typically analyzed using plots of (x, t) and (x^2, t), respectively, and in these cases the slopes, k, will be proportional to $b^{1/2}$ and b. Indeed, examining the exact Bousanquet solution for capillary-driven imbibition, Eq. (31), which describes horizontal channels over all times, T, and approximately vertical channels at times $T < T_c$, shows that the contact angle dependence in $x^2(t)$ arises from an overall factor proportional to b. Thus, if we write $x^2(t) = bf(a, t)$ where $f(a, t)$ is a function not involving the contact angle, a plot of $x^2(t)$ versus $f(a, t)$ will have a slope of $k = b$. The sensitivity of the slope, k, to small changes in the contact angle can be evaluated as a fractional error in the slope on these plots. For the case of closed and open channels with the same contact angle on each surface, the error in the slope for the Lucas–Washburn and Bousanquet plots is,

$$\left|\frac{\delta k}{k}\right| \Big/ \delta\theta = \left|\frac{\delta b}{b}\right| \Big/ \delta\theta = \begin{cases} \tan\theta_e \\ (2\varepsilon+1)\sin\theta_e / [(2\varepsilon+1)\cos\theta_e - 1] \end{cases} \quad (48)$$

As shown by Fig. 7, the error given by Eq. (48) as a percentage change in slope per degree is large and changes rapidly for contact angles close to the transition to imbibition; a small uncertainty in contact angle results in large changes in the slope and hence estimates of b from experimental data. Experimentally, for open channels there is therefore an incentive to work with liquids that wet the surfaces effectively and therefore have contact angles

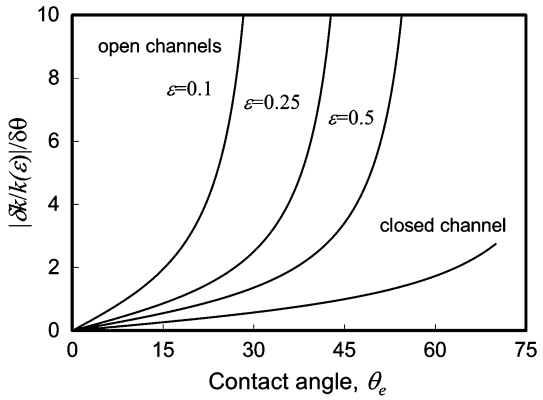

Fig. 7 The sensitivity of the fractional change in slope per degree in the Lucas–Washburn equation to small changes in contact angle for *closed* and *open rectangular* channels; aspect ratios of $\varepsilon = 0.1$, 0.25 and 0.5 are shown

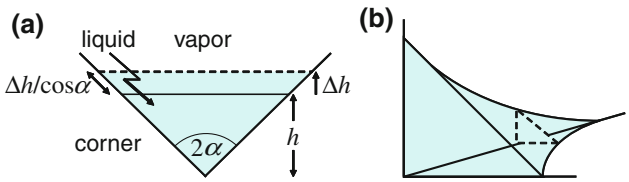

Fig. 8 Surface free energy changes as a tube/slab of liquid penetrates into a channel resulting in new solid–liquid and liquid–vapor interfaces. **a** Two-dimensional corner viewpoint, and **b** an edge viewed as a sequence of two-dimensional corners

below that determined by the critical angle for imbibition arising from the aspect ratio. However, this then leads to increasing risks that the assumption that imbibition occurs in a tube like manner with a meniscus of constant profile will not be accurate as discussed below.

Rectangular and many other cross-sectional shape channels differ in their wetting properties from flat and smoothly circular surfaces, precisely because two walls meet at an angle. This effect, the corner filling condition, can be understood by a simple two-dimensional model. Consider two walls joining at an angle 2α with a liquid initially partially filling the corner to a depth h (Fig. 8a). When the corner fills with liquid by an additional amount Δh, the surface free energy change is given by,

$$\Delta F = 2\Delta h\left[\frac{(\gamma_{SL} - \gamma_{SV})}{\cos\alpha} + \gamma_{LV}\tan\alpha\right] = \frac{2\Delta h\gamma_{LV}}{\cos\alpha}[\sin\alpha - \cos\theta_e] \quad (49)$$

where Young's law has been used to replace the combination of interfacial tensions by $\cos\theta_e$. Thus, the change in surface free energy is zero or negative whenever $\cos\theta_e \geq \sin\alpha$, which gives,

$$(\alpha + \theta_e) \leq 90^\circ \quad (50)$$

as the corner filling condition. In the case of a flat surface, $\alpha = 90°$ and a surface wets when the contact angle vanishes, and. in the case of parallel plates, $\alpha = 0°$ and the surface wets between the plates whenever $\theta_e \leq 90°$. Thus, Eq. (46), which is the condition for imbibition assuming a tube of liquid advancing in a channel, must be considered alongside Eq. (50).

Whilst this was a two-dimensional argument, an edge can be viewed as a sequence of two-dimensional corners (Fig. 8b) and so the same condition, Eq. (50), will apply. For example, for the open rectangular channel the side walls meet the bottom surface at 90° so that the corner filling condition is $\theta_e \leq 45°$, whereas Eq. (47) suggests imbibition will only occur for channel aspect ratios, ε, larger than 0.207. Thus, fingers of liquid can imbibe into open channels at aspect ratios lower than might otherwise be expected. Bico and Quéré (2002) have shown that corner filling leads in square cross-section capillary tubes to fingers of liquid rising along the internal edges against gravity in advance of the central meniscus, which itself rises to an equilibrium height which is a factor $(2 + \pi^{1/2})/4$ less than would be the case without the fingers. Moreover, Ponomarenko et al. (2011) have recently used scaling arguments to show that in the viscous regime of capillary rise against gravity and independent of specifics of the geometry, the fingers spread faster than the main meniscus, which follows a Lucas–Washburn law.

Thus, for good capillary-driven imbibition in open and closed rectangular channels with reduced sensitivity to the precise value of contact angle, Eq. (46) implies it is better to use low contact angle liquids. However, doing so is likely to lead to increasingly stronger effects from liquid fingers spreading along the edges between walls at lower contact angles and higher intrusion rates. From the point of view of microfluidics and lab-on-a-chip, the consequences of this are potentially serious with fingers of liquid spontaneously spreading in advance of the bulk liquid and potentially causing contamination. An interesting question is whether the capillary-drive imbibition/rise in open and closed rectangular channels of the main meniscus can still be accurately described by Eqs. (31) and (34). The experimental consideration of this is given in Sect. 4.

3 Experimental methods

To test the theory on the influence of capillary shape experiments were conducted on the capillary rise of polydimethylsiloxane (PDMS) oils in three cross-sectional geometries, circular glass capillary tubes, square glass capillary tubes, and SU8 open rectangular cross-section channels. The liquid–air interface in open channels is essentially completely hydrophobic/oleophobic and so a strongly wetting liquid, such as PDMS with its low equilibrium contact angle ($\theta_e = 0$) is needed to ensure complete wetting. This choice also eliminates any sensitivity to the precise value of θ_e for liquid penetration into open channels discussed in Sect. 2.3. For each geometry, four PDMS oils (Dow Corning Xiameter PMX-200) of viscosities $\eta = 96.0$, 48.0, 19.2 and 4.8 mPa s (±5 %) and corresponding densities of 960, 950, 930 and 913 kg m^{-3} were investigated. The surface tension of these oils is constant at 19.8 mN m^{-1}. The details of the tubes/channels used are given in Table 1.

Table 1 Physical dimensions of channels and experimental parameters

Channel	Size (μm)	Aspect ratio ($\varepsilon = H/W$)
Circular glass tube	$R = 650$	–
Glass square tube	$H \times W = 600 \times 600$	1
	$H \times W = 400 \times 400$	1
SU8 open rectangular channels	$H \times W = 135^a \times 600^b$	0.225
	$H \times W = 135^a \times 400^b$	0.338

[a] ±5 μm

[b] ±5 μm

The open SU8 channels were fabricated on glass slides using photolithography. After a slide was cleaned, a 20 μm thick SU8 base layer (SU8-10 MicroChem) was spin-coated, pre-baked (65 °C for 2 min then at 95 °C for 2 min), UV exposed through a mask, and then post-baked at 65 °C for 30 min. A second SU8 layer (SU8-50 MicroChem), of a nominal thickness of 135 μm, was then spin-coated, pre-baked, UV exposed and then post-baked (65 °C for 30 min then at 95° C for 30 min) to form the side walls of the channels; this ensured that all three faces of the channels were constructed of SU8. The photoresist was then developed to leave open rectangular channels. The depths of the channels were measured with a stylus profilometer. Variability in the depths of the channels was observed between samples. The data presented in this report are for channels with depths in the range 130-140 μm, and for each channel the measured depth value is used when comparing the data with theory. Commercially available square glass capillary tubes of sides 400 μm and 600 μm were also used in the experiments together with a 650 μm radius circular glass capillary tube for calibration and comparison. SEM characterisations found the internal wall surfaces of the circular and square glass capillaries to be smooth and free from striations.

Each tube/channel was cleaned in isopropylalcohol (IPA) and dried at 100 °C for 1 h prior to measurements.

A small amount of blue dye was used to increase contrast; control experiments without the dye did not show any differences in the dynamics of capillary rise. The sample was mounted vertically next to a rectangular grid which provided a length calibration. PDMS oil from a large reservoir was brought up into contact with the tube/channel very slowly until spontaneous filling started. A high speed camera (NAC Hotshot 512SC) was used to capture videos of the rise of the liquid at 50 frames per second. The videos were analyzed after the experiment and the position of the central meniscus measured in ImageJ from the corresponding frames at a set of predetermined time intervals. The initial time $t = 0$ was defined as the time the liquid first appeared to enter the tube/channel; this was determined to within one frame (i.e., 20 ms). The spatial resolution can be estimated from the field of view of the camera and the pixel resolution and is around 0.02 mm. Each sample/tube was used once only, but measurements were repeated on samples with the same physical dimensions several times and under the same conditions to check for reproducibility.

4 Results and discussions

As discussed in Sect. 2.3, flow in non-circular channels can be expected to be accompanied by advancing liquid fingers that develop with time, increase in prominence and progress ahead of the main meniscus of the liquid. These fingers were visible in the closed square glass tubes (with aspect ratio $\varepsilon = 1$) along all four of the internal edges defined by were two walls meet at 90°. These liquid fingers were very thin and confined to the edges where the walls of the tubes meet making them difficult to clearly image in our experimental set up (Fig. 9a). These observations are consistent with those of Girardo et al. (2009) for similar aspect ratio, but in open channels. In contrast, the fingers in our open rectangular SU8 channels with aspect ratios $\varepsilon = 0.225$ and 0.338, which propagated along the internal edges defined by where the bottom of the channel and a side wall meet, were very prominent and extended far beyond the main meniscus of the liquid (Fig. 9b). They were found to progress much faster than the main front of the liquid, to such an extent as to eventually exit from the end of the channels completely. The dependence of the shape of the fingers on ε is consistent with the measurements of Seemann et al. (2005) of static liquids in open rectangular channels, who found that their shape was determined by contact angle and aspect ratio, and that, for completely wetting liquids ($\theta_e = 0$), thick and extended fingers occurred when the height of channels was sufficiently small compared to their width for $\varepsilon < 0.5$, whereas thin fingers, restricted to the corners of the channels, were observed for $\varepsilon > 0.5$.

Fig. 9 Micrographs of the shapes of the meniscus of the liquid in rectangular channels/tubes. The *arrows* show liquid fingers which develop with time and advance ahead of the main meniscus. **a** Closed square tubes: fingers are thin and are confined to the four edges where the walls of the tube meet. **b** Open rectangular channels with $\varepsilon = 0.225$ (also 0.338): fingers are thick and extended and propagate along the internal edges defined by where the bottom of the channel and a side wall meet

In our experimental conditions, the cross-over time for the imbibition of the main body of liquid above which the visco-gravitational solution is a better approximation than the Bousanquet solution (discussed in Sect. 2.2) occurs within the first 25 ms after liquids enter the tubes/channels for all viscosities, which, in all our measurements, takes place within the first measurement time interval. The viscous-gravitational solution is, therefore, the best analytical approximation for our experiments. For each measurement, the variation of the position of the meniscus with time was fitted to both the exact numerical solution [Eq. (25)] and analytical solution [eq. (35) with $\varphi = 90°$]. Both fits were performed within Mathematica® (Wolfram research) using three fitting parameters, a, b and t_0, where the viscous coefficient (a) and capillary coefficient (b) are defined by Eq. (26) and Eq. (28), respectively. Fitting at the very early stages of imbibition was found to be sensitive to the initial time offset parameter t_0 which was, in practice, found to be less than one to, occasionally, two measurement time intervals. In all fits, a constant contact angle value of $\theta_e = 0$ was assumed, and for the open rectangular channels

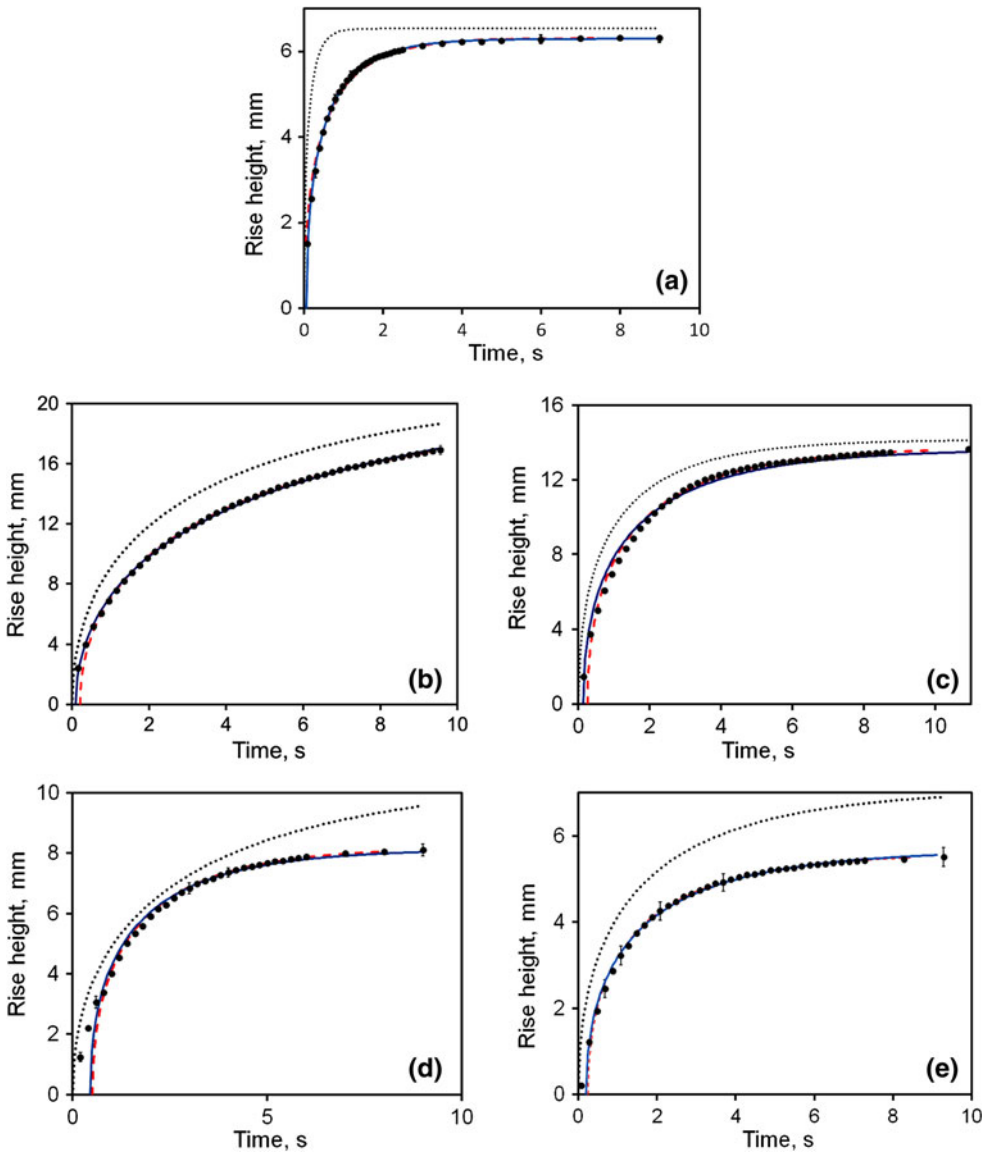

Fig. 10 The variation of the rise height with time of the 19.2 mPa s oil in: **a** 650 μm radius glass tube, **b** 400 μm square tube, **c** 600 μm square tube, **d** 400 μm open channel and **e** 600 μm open channel. The *solid symbols* represent the experimental data and the *solid* and *dashed lines* the numerical and analytical fits respectively. The *dotted lines* give the expected rise using the nominal device parameters

data analysis was restricted to the part of the experiment during which the wetting fingers remained in the channels.

The solid symbols in Fig. 10 show the variation with time (t) of the capillary rise height (x) of the 19.2 mPa s oil in (a) 650 μm radius glass tube, (b) 400 μm square tube, (c) 600 μm square tube, (d) 400 μm open microchannel, and (e) 600 μm open microchannel. The data show good reproducibility in circular and square tubes. However, some variability between samples (up to 10 %) was observed for open channels. The most likely reason for this is the variation in depth of the channels between samples. The solid lines in Fig. 10 are the numerical solutions [Eq. (25)], whilst the dashed lines are the fits obtained using the approximate visco-gravitational solution [Eq. (35)]. The data can be fitted accurately (to within 5 %) using both solutions, albeit a discrepancy at the very early stage of imbibition (seen in Fig. 10c, d e). This is, perhaps, not surprising since our analysis assumes a constant contact angle and does not take into account of any dynamic contact angle changes during the initial entry into the tubes/channels. Moreover, the parameters obtained from fitting using the exact numerical solution and the approximate analytical visco-gravitational solution agree to within 10 % for the viscous coefficient a and 3 % for the capillary coefficient b. Thus, either the numerical or the visco-gravitational solution can be used to fit the position of the meniscus for our closed tubes and open channels. Moreover, the existence of liquid fingers advancing ahead of the main meniscus of liquid do not seem to prevent the theory from describing the advance of the meniscus for the main body of liquid for values of channel aspect ratio ε considered in our work.

In our experiments, we found that the equilibrium capillary rise height was broadly consistent with expectations using the nominal device parameters. The value of the capillary parameter b obtained from the fits agrees very well (to within 2 % for circular cross-section tubes) with the experimental observations of the equilibrium height rise x_e ($b = x_e g$). However, the rate at which the liquid approached this equilibrium was always slower than predicted by theory, as is illustrated by the dotted curves in Fig. 10, which represent the expected rise. The value of the viscous coefficient a is larger than predicted by theory for all viscosities and most all tubes and channels except for the 400 μm open channels. We found this parameter to be around 4.2 (±0.2) times larger than the theoretical value for circular tubes and around 1.5 (±0.1) and 1.3 (±0.1) times larger than the theoretical value for 600 and 400 μm closed square capillaries, respectively. For the 600 and 400 μm wide open channels the fitted values of the viscous coefficient a is around 1.5 (±0.2) and 0.9 (±0.1) times the value predicted from the theory. Preliminary measurements on smaller radius circular cross-section capillary tubes suggests there is a better agreement between fitted and predicted values as the radius reduces to less than a tenth of the capillary length of the liquid. The data for the square tubes and rectangular channels also indicate a better agreement for smaller dimensions with a reasonable agreement for the 400 μm wide open channels.

Retardation of liquid rise in capillaries and tubes has previously been reported by other authors who have suggested a range of possible reasons. These include a possible dynamic contact angle effect during flow (Siebold et al. 2000; Hamraoui and Nylander 2002; Chebbi 2007; Xiao et al. 2006; Xue et al. 2006), and a possible retardation coefficient arising from an increased frictional dissipation of the moving liquid front (Hamraoui and Nylander 2002). A number of different models for how $\cos\theta_e$ in the capillary term b in Eq. (28), hence in Eq. (25), might be replaced by a dynamic $\cos\theta$ and how that would relate to dissipation were considered in detail by Popescu et al. (2008). They considered four models for a dynamic contact angle including both hydrodynamic (Hoffman 1975; de Gennes 1985; Cox 1986) and molecular-kinetic theory (Blake and Haynes 1969). In the Hoffman-de Gennes (HdG) approach, the dynamic contact angle, $\theta(t)$, edge speed, dx/dt, relationship is,

$$\left(\frac{dx}{dt}\right) \approx kv^*\theta(t)(\cos\theta_e - \cos\theta(t)) \tag{51a}$$

where k is a constant determined by viscous dissipation and $v^* = \gamma_{LV}/\eta$ is characteristic velocity determined by the ratio of surface tension to viscosity. For the linearized form of the molecular-kinetic theory (MKT) model the analogous relationship is,

$$\left(\frac{dx}{dt}\right) = \xi^{-1}v^*(\cos\theta_e - \cos\theta(t)) \tag{51b}$$

where the combination $\xi^{-1}v^*$ is a coefficient related to wetting line friction, which depends on both fluid viscosity and solid–liquid interaction (Bertrand et al. 2009; Stukan et al. 2010). If we focus on cylindrical tubes and use $\cos\theta(t)$ from Eq. (51a, 51b) in Eq. (28) rather than $\cos\theta_e$ to obtain a parameter b_d using the dynamic contact angle, i.e.,

$$\text{(HdG model) } b \to b_d = 2\gamma_{LV}\cos\theta/\rho R = \frac{2\gamma_{LV}}{\rho R}\left[\cos\theta_e - \frac{1}{kv^*\theta}\left(\frac{dx}{dt}\right)\right] \tag{52a}$$

and

$$\text{(MKT model) } b \to b_d = 2\gamma_{LV}\cos\theta/\rho R = \frac{2\gamma_{LV}}{\rho R}\left[\cos\theta_e - \frac{1}{\xi^{-1}v^*}\left(\frac{dx}{dt}\right)\right] \tag{52b}$$

there then arises an additional velocity-dependent term. Interestingly, when the dynamic parameter b_d is used in Eq. (25) rather than the equilibrium parameter b, the effect can be viewed as retaining the original equilibrium b parameter, but replacing the a parameter by a dynamic a_d parameter,

$$\text{(HdG model) } a \to a_d = a\left[1 + \left(\frac{R}{4x(t)}\right)\left(\frac{1}{k\theta(t)}\right)\right] \tag{53a}$$

or

$$\text{(MKT model) } a \to a_d = a\left[1 + \left(\frac{R}{4x(t)}\right)\xi\right] \tag{53b}$$

The additional term in Eq. (53a, 53b) is time-dependent and vanishes as the imbibition progresses and the dynamic contact angle relaxes to its equilibrium value. This type of term can be expected to cause a slower approach to equilibrium than might be expected from Eq. (25) using only a constant contact angle approximated by the equilibrium contact angle. This is consistent with the numerical investigation of Popescu et al. (2008) and with physical expectations that when a vertical tube first comes into contact with the horizontal meniscus of the reservoir the instantaneous contact angle is likely to be 90° and must relax towards the equilibrium value as imbibition commences. This is also consistent with our preliminary observations that agreement of the fitted a parameter with theoretical expectations improves as the radius of the tube decreases. A similar argument should apply to square capillaries and open channels.

In our case, it is also possible that some of the increased viscous dissipation in the rectangular channels could be induced by the wetting fingers and that their contributions

may be dependent on the size and/or aspect ratio ε of the channels. However, Girardo et al. (2012) found that fingers do not seem to induce appreciable extra dissipation in the early stage of microcapillary imbibitions in horizontally mounted smooth microchannels. It is also of note that the fitted values of the viscous coefficient a for the open channels are a factor 2 and 3 lower (for the 400 and 600 μm wide open channels) than would be expected for a rigidified liquid–air boundary, as required by Yang et al. (2011) to explain the dynamics of capillary flow in their horizontally mounted open narrow microchannels. This indicates that a non-rigidified liquid–air interface best represents the flow in our lower aspect ratio channels. A further detailed quantitative investigation would be needed to clarify the dependence of the viscous coefficient on channel size and aspect ratio on dissipation, but this is beyond the scope of our report.

Whilst the measured equilibrium rise height values are to within 2 % of the predicted theoretical value for the circular cross-section tubes, they are around 5 % smaller than theoretical predictions for square tubes. We attribute this reduction to the wetting fingers, which are predicted to reduce the equilibrium height by a value of $(2 + \pi^{1/2})/4 = 0.943$ in square geometries (Bico and Quéré 2002). The equilibrium height is, however, a factor of 0.83 (±0.03) times smaller than theory for the open channels, although confidence in the exact factor requires some caution since the data has considerable scatter. This is, perhaps, not surprising since the fingers are more prominent, and so may induce a larger reduction in the equilibrium height (Bico and Quéré 2002).

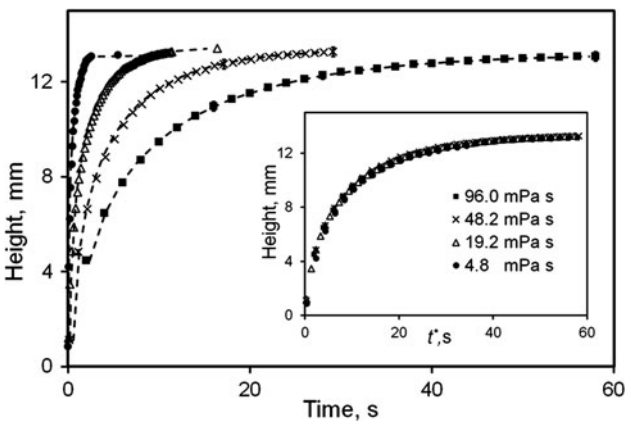

Fig. 11 The effect of viscosity on capillary rise for the 600 μm square tube. The *dashed lines* are the expected rise obtained by taking the fitted value of a for the 96.0 mPa s sample and scaling it according to the ratio of viscosities. The *inset* shows the data scaled for viscosity. The scaled time $t^* = 96t/\eta$

Figure 11 shows the effect of viscosity on the capillary rise in a square tube with sides of 600 μm. As expected, the rise is faster for the lower viscosity oils, but the equilibrium rise height $x_e = b/g$ remains constant as it is independent of viscosity. For the same physical geometry, the visco-gravitational solution predicts that, at a given rise height x, $t \propto ab \propto \eta$ [Eq. (35), and Eqs. (26) and (28)]. It should, therefore, be possible to scale from one viscosity value to another provided the density and surface tension of the liquid are independent of viscosity, which is the case for our liquids to within 5 %. To verify this experimentally, the data in Fig. 11 are re-plotted with the time for each viscosity data scaled to that of the 96.0 mPa s sample by multiplying it by a factor equal to $96/\eta$ ($t^* = t \times 96/\eta$); the results are shown in the inset to Fig. 11. It can be seen that the data scale with viscosity, supporting the above argument. Moreover, this indicates that liquid rise can be predicted for any viscosity value from the experimental data of one given viscosity (taken here to be the 96 mPa s) by scaling the value of a, obtained from the fit to the analytical visco-gravitational solution, according to the ratio of viscosities (dashed lines in Fig. 11). Similar results were obtained for 400 μm square tubes (Fig. 12a) and round capillaries (Fig. 12b). However, our data for the open rectangular channels do not scale as well with viscosity (Fig. 12c, d). We believe this is due to the variations in the height of channels (130–140 (±5) μm) from one sample to another that were difficult to prevent during their fabrication. An improved scaling is obtained (as shown in the insets of Fig. 12c, d) if we account for the variations in channel depths between samples at a given channel width as explained in the next paragraph.

The inset of Fig. 13 shows the data from Fig. 10b, c re-plotted to show the effect of the tube dimension on the liquid rise in square tubes ($H = W$) for the 96 mPa s oil. As expected the equilibrium rise height $x_e = b/g$ scales inversely proportional to H [Eq. (28)]. For a given x/x_e, the visco-gravitational solution [Eq. (35)] predicts $t \propto ab \propto \eta/(H^3\zeta_c(\varepsilon)) \propto \eta H^{-3}$, where $\zeta_c(\varepsilon) = \zeta_c(1)$ is independent of dimension for square tubes. It should, therefore, be possible to scale liquid rise of any sample of dimension H relative to any other given dimension (say 400 μm) both for rise height and time by multiplying x by $H/400$ and time by $(H/400)^3$. Moreover, time can also be scaled for viscosity in the same way as performed above (Figs. 11, 12a). The results are shown in Fig. 13. It is evident that the data cannot be fully scaled for sample dimensions. The reason for this is that theory underestimates viscous dissipation by an amount that is dependent on sample dimension as discussed above. For open channels of varying depths and with $\theta_e = 0$, $t \propto ab \propto \eta\varepsilon/(H^3\zeta_o(\varepsilon)) \propto \eta/(WH^2\zeta_o(\varepsilon))$, where $\zeta_o(\varepsilon)$ can be determined using Eq. (23). So it should

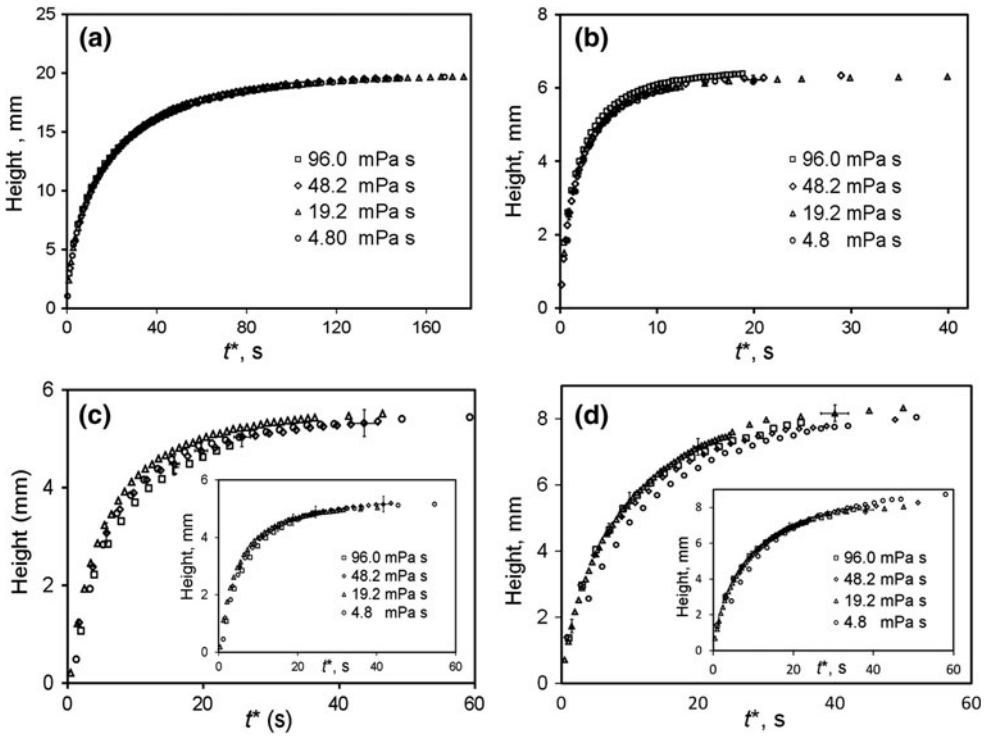

Fig. 12 Capillary rise scaled for viscosity in: **a** 400 μm square tube, **b** $R = 650$ μm circular tube, **c** 600 μm open channel and **d** 400 μm open channel. The *insets* to **c** and **d** show the data scaled to account for depth variations between samples

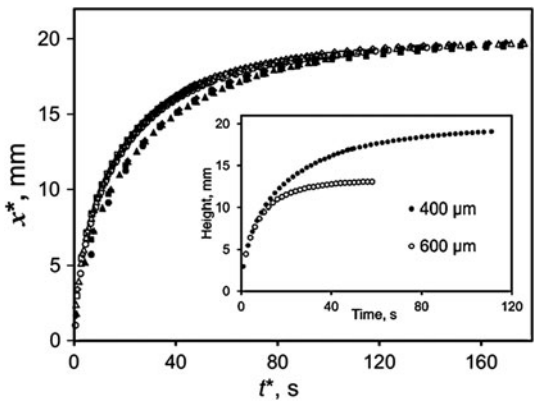

Fig. 13 The capillary rise in square tubes scaled for tube dimension and viscosity for 400 μm (*empty symbol*) and 600 μm (*filled symbol*). The scaled rise height $x^* = (Hx/400)$ and scaled time $t^* = (H/400)^3 t$. The *inset* shows the effect of the dimension of square tube on the capillary rise for the 96.0 mPa s oil

also be possible, in principle, to scale the liquid rise for any sample of known width W, height H (hence ε) and viscosity η relative any other sample with given dimensions and viscosity following the same procedure as for square capillaries. The data can be scaled for viscosity and small variations in channel depths at fixed channel widths (insets of Fig. 12c, d); however, the data cannot be fully scaled for channel width, in the same way as for closed square capillaries, because of the dimension-dependent retardation discussed above.

5 Conclusions

In this work, we have presented the theory for capillary-driven imbibition into tubes of circular and square cross-sections and into open and closed rectangular channels in a common formalism. The theory can describe tubes and channels at any angle to the horizontal from horizontal to vertical. We have shown that there is a cross-over time and imbibition length below which the exact numerical solution of the equations is best described by the analytical Bousanquet solution and above which by the analytical visco-gravitational solution. We have also highlighted that corner filling wetting ideas lead to the expectation of liquid fingers advancing in square and rectangular tubes and channels in advance of the main meniscus and we have observed this to be the case experimentally. Nonetheless, the theory accurately describes the form of the observed imbibition for capillary rise of PDMS oils in closed square and open rectangular channels of different width cross-sections. We found that the analytical viscous-gravitational solution as an approximation of the exact differential equation for capillary imbibition can be adequately used to fit capillary rise in the systems we studied. From these fits, we found that the viscous friction coefficient is larger than predicted by theory, but that agreement improves for smaller dimension samples, and we attribute this to dynamic contact angle effects. The data indicate that the shapes of the wetting fingers are dependent on the aspect ratio of the samples. For our completely wetting liquids

($\theta_e = 0$), the liquid fingers are thin and form near the corner edges for square tubes with aspect ratio $\varepsilon = 1$, whereas they are prominent for open channels with low values of ε (0.225, 0.338), in agreement with observations on static fluids. These fingers may have important implications for the design and performance of microfluidic devices based on liquid imbibition of wetting liquids with contact angles $\theta_e \leq 45°$ in rectangular microchannels. It is possible that they might affect the amount and dynamics of liquid flow, cause contamination between the micro-compartments or connect, what would otherwise be, separate area of liquids.

Acknowledgments The authors acknowledge financial assistance from the UK Engineering and Physical Sciences Research Council (Grant No. EP/E063489/1). HJ would like to acknowledge Nottingham Trent University for financial support.

References

Ahadian S, Mizuseki H, Kawazoe Y (2009) An efficient tool for modeling and predicting fluid flow in nanochannels. J Chem Phys 131:184506. doi:10.1063/1.3253701

Ayyaswamy PS, Catton I, Edwards DK (1974) Capillary flow in triangular grooves. J Appl Mech 41:332–336. doi:10.1115/1.3423288

Baret J-C, Decré MMJ, Herminghaus S, Seemann R (2007) Transport dynamics in open microfluidic grooves. Langmuir 23:5200–5204. doi:10.1021/la063584c

Bertrand E, Blake TD, de Coninck J (2009) Influence of solid-liquid interactions on dynamic wetting: a molecular dynamics study. J Phys: Condens Matter 21:464124. doi:10.1088/0953-8984/21/46/464124

Bico J (2000) Mécanismes d' imprégnation: surfaces texturées, Bigouttes, Poreux. PhD thesis, Université de Paris VI

Bico J, Quéré D (2002) Rise of liquids and bubbles in angular capillary tubes. J Colloid Interface Sci 247:162–166. doi:10.1006/jcis.2001.8106

Bico J, Quéré D (2003) Precursors of impregnation. Europhys Lett 61:348–353. doi:10.1209/epl/i2003-00196-9

Bico J, Thiele U, Quéré D (2002) Wetting of textured surfaces. Colloids Surf A 206:41–46. doi:10.1016/S0927-7757(02)00061-4

Blake TD, Coninck J (2004) The influence of pore wettability on the dynamics of imbibition and drainage. Colloids Surf A 250:395–402. doi:10.1016/j.colsurfa.2004.05.024

Blake TD, Haynes JM (1969) Kinetics of liquid/liquid discplacement. J Colloid Interface Sci 30:421–423. doi:10.1016/0021-9797(69)90411-1

Bouaidat S, Hansen O, Bruus H et al (2005) Surface-directed capillary system; Theory, experiments and applications. Lab Chip 5:827–836. doi:10.1039/b502207j

Bousanquet C (1923) On the flow of liquids into capillary tubes. Philos Mag Ser 6(45):525–531. doi:10.1080/14786442308634144

Brody JP, Yager P, Goldstein RE, Austin RH (1996) Biotechnology at low Reynolds numbers. Biophys J 71:3430–3441. doi:10.1016/S0006-3495(96)79538-3

Byon C, Kim SJ (2011) The effect of meniscus on the permeability of micro-post arrays. J Micromech Microeng 21:115011. doi:10.1088/0960-1317/21/11/115011

Chebbi R (2007) Dynamics of liquid penetration into capillary tubes. J Colloid Interface Sci 315:255–260. doi:10.1016/j.jcis.2007.06.073

Chen Y, Melvin LS, Rodriguez S et al (2009) Capillary driven flow in micro scale surface structures. Microelectron Eng 86:1317–1320. doi:10.1016/j.mee.2009.02.016

Clime L, Brassard D, Pezacki JP, Veres T (2012) Self-priming of liquids in capillary autonomous microfluidic systems. Microfluid Nanofluid 12:371–382. doi:10.1007/s10404-011-0881-7

Concus P, Finn R (1969) On the behavior of a capillary surface in a wedge. Proc Natl Acad Sci USA 63:292–299. doi:10.1073/pnas.63.2.292

Cox RG (1986) The dynamics of the spreading of liquid on a solid-surface. 1. Viscous-flow. J Fluid Mech 168:169–194. doi:10.1017/S0022112086000332

Darhuber A, Troian S, Reisner W (2001) Dynamics of capillary spreading along hydrophilic microstripes. Phys Rev E 64:1–8. doi:10.1103/PhysRevE.64.031603

de Gennes PG (1985) Wetting—statics and dynamics. Rev Mod Phys 57:827–863. doi:10.1103/RevModPhys.57.827

Dong M, Chatzis I (1995) The imbibition and flow of a wetting liquid along the corners of a square capillary tube. J Colloid Interface Sci 172:278–288. doi:10.1006/jcis.1995.1253

Fries N, Dreyer M (2008a) The transition from inertial to viscous flow in capillary rise. J Colloid Interface Sci 327:125–128. doi:10.1016/j.jcis.2008.08.018

Fries N, Dreyer M (2008b) An analytic solution of capillary rise restrained by gravity. J Colloid Interface Sci 320:259–263. doi:10.1016/j.jcis.2008.01.009

Fries N, Dreyer M (2009) Dimensionless scaling methods for capillary rise. J Colloid Interface Sci 338:514–518. doi:10.1016/j.jcis.2009.06.036

Girardo S, Cingolani R, Chibbaro S, Diotallevi F, Succi S, Pisignano D (2009) Corner liquid imbibitions during capillary penetration in lithographically made microchannels. Appl Phys Lett 94:171901–171903. doi:10.1063/1.3123804

Girardo S, Palpacelli S, De Maio A, Cingolani R, Succi S, Pisignano D (2012) Interplay between shape and roughness in early stage microcapillary imbibition. Langmuir 28:2596–2603. doi:10.1021/la2045724

Hamraoui A, Nylander T (2002) Analytical approach for the Lucas–Washburn equation. J Colloid Interface Sci 250:415–421. doi:10.1006/jcis.2002.8288

Hamraoui A, Thuresson K, Yaminsky V, Nylander T (2000) Can a dynamic contact angle be understood in terms of a friction coefficient? J Colloid Interface Sci 226:199–204. doi:10.1006/jcis.2000.6830

Han A, Mondin G, Hegelbach NG et al (2006) Filling kinetics of liquids in nanochannels as narrow as 27 nm by capillary force. J Colloid Interface Sci 293:151–157. doi:10.1016/j.jcis.2005.06.037

Hoffman RL (1975) Study of advancing interface. 1. Interface shape in liquid-gas systems. J Colloid Interface Sci 50:228–241. doi:10.1016/0021-9797(75)90225-8

Ichikawa N, Hosokawa K, Maeda R (2004) Interface motion of capillary-driven flow in rectangular microchannel. J Colloid Interface Sci 280:155–164. doi:10.1016/j.jcis.2004.07.017

Ishino C, Reyssat M, Reyssat E et al (2007) Wicking within forests of micropillars. Europhys Lett. doi:10.1209/0295-5075/79/56005

Jokinen V, Franssila S (2008) Capillarity in microfluidic channels with hydrophilic and hydrophobic walls. Microfluid Nanofluid 5:443–448. doi:10.1007/s10404-008-0263-y

Jong W, Kuo T, Ho S et al (2007) Flows in rectangular microchannels driven by capillary force and gravity. Int Commun Heat Mass Transfer 34:186–196. doi:10.1016/j.icheatmasstransfer.2006.09.011

Krotov VV, Rusanov AI (1999) Physicochemical hydrodynamics of capillary systems. Imperial College Press, p 222

Kusumaatmaja H, Pooley CM, Girardo S et al (2008) Capillary filling in patterned channels. Phys Rev E 77:3–6. doi:10.1103/PhysRevE.77.067301

Legait B (1983) Laminar flow of two phases through a capillary tube with variable square cross-section. J Colloid Interface Sci 96:28–38. doi:10.1016/0021-9797(83)90005-X

Liou WW, Peng Y, Parker PE (2009) Analytical modeling of capillary flow in tubes of nonuniform cross section. J Colloid Interface Sci 333:389–399. doi:10.1016/j.jcis.2009.01.038

Liu W, Li Y, Cai Y, Sekulic DP (2011) Capillary rise of liquids over a microstructured solid surface. Langmuir 27:14260–14266. doi:10.1021/la2033884

Lucas R (1918) Ueber das Zeitgesetz des Kapillaren Aufstiegs von Flussigkeiten. Kolloid Z 23:15–22. doi:10.1007/BF01461107

Marmur A, Cohen RD (1997) Characterization of porous media by the kinetics of liquid penetration: the vertical capillaries model. J Colloid Interface Sci 189:299–304. doi:10.1006/jcis.1997.4816

McHale G, Shirtcliffe NJ, Aqil S et al (2004) Topography driven spreading. Phys Rev Lett 93:1–4. doi:10.1103/PhysRevLett.93.036102

Mehrabian H, Gao P, Feng JJ (2011) Wicking flow through microchannels. Phys Fluids 23:122108. doi:10.1063/1.3671739

Mognetti BM, Yeomans JM (2009) Capillary filling in microchannels patterned by posts. Phys Rev E 80:1–8. doi:10.1103/PhysRevE.80.056309

Mumley TE, Radke C, Williams MC (1986) Kinetics of liquid/liquid capillary rise: I. Experimental observations. J Colloid Interface Sci 109:398–412. doi:10.1016/0021-9797(86)90318-8

Oh JM, Faez T, Beer S, Mugele F (2009) Capillarity-driven dynamics of water–alcohol mixtures in nanofluidic channels. Microfluid Nanofluid 9:123–129. doi:10.1007/s10404-009-0517-3

Ponomarenko A, Quéré D, Clanet C (2011) A universal law for capillary rise in corners. J Fluid Mech 666:146–154. doi:10.1017/S0022112010005276

Popescu MN, Ralston J, Sedev R (2008) Capillary rise with velocity-dependent dynamic contact angle. Langmuir 24:12710–12716. doi:10.1021/la801753t

Quéré D (1997) Inertial capillarity. Europhys Lett 39:533–538. doi:10.1209/epl/i1997-00389-2

Quéré D (2008) Wetting and roughness. Annu Rev Mater Res 38:71–99. doi:10.1146/annurev.matsci.38.060407.132434

Ramé E, Weislogel MM (2009) Gravity effects on capillary flows in sharp corners. Phys Fluids 21:042106. doi:10.1063/1.3109685

Ransohoff T, Radke CJ (1988) Laminar flow of a wetting liquid along the corners of a predominantly gas-occupied noncircular pore. J Colloid Interface Sci 121:392–401. doi:10.1016/0021-9797(88)90442-0

Reyssat M, Courbin L, Reyssat E, Stone HA (2008) Imbibition in geometries with axial variations. J Fluid Mech 615:335–344. doi:10.1017/S0022112008003996

Romero LA, Yost FG (2006) Flow in an open channel capillary. J Fluid Mech 322:109–129. doi:10.1017/S0022112096002728

Rosendahl U, Ohlhoff A, Dreyer ME (2004) Choked flows in open capillary channels: theory, experiment and computations. J Fluid Mech 518:187–214. doi:10.1017/S0022112004001041

Schoelkopf J, Gane PAC, Ridgway CJ, Matthews GP (2002) Practical observation of deviation from Lucas–Washburn scaling in porous media. Colloids Surf 206:445–454. doi:10.1016/S0927-7757(02)00066-3

Seemann R, Brinkmann M, Kramer EJ, Lange FF, Lipowsky R (2005) Wetting morphologies at microstructured surfaces. Proc Natl Acad Sci USA 102:1848–1852. doi:10.1073/pnas.0407721102

Shirtcliffe NJ, McHale G, Newton MI et al (2006) Critical conditions for the wetting of soils. Appl Phys Lett 89:094101. doi:10.1063/1.2339072

Shirtcliffe NJ, McHale G, Atherton S, Newton MI (2010) An introduction to superhydrophobicity. Adv Colloid Interface Sci 161:124–138. doi:10.1016/j.cis.2009.11.001

Siebold A, Nardin M, Schultz J et al (2000) Effect of dynamic contact angle on capillary rise phenomena. Colloids Surf A 161:81–87. doi:10.1016/S0927-7757(99)00327-1

Squires T, Quake SR (2005) Microfluidics: fluid physics at the nanoliter scale. Rev Mod Phys 77:977–1026. doi:10.1103/RevModPhys.77.977

Srivastava N, Din C, Judson A et al (2010) A unified scaling model for flow through a lattice of microfabricated posts. Lab Chip 10:1148–1152. doi:10.1039/b919942j

Stange M, Dreyer ME, Rath HJ (2003) Capillary driven flow in circular cylindrical tubes. Phys Fluids 15:2587–2601. doi:10.1063/1.1596913

Staples TL, Shaffer DG (2002) Wicking flow in irregular capillaries. Colloids Surf A 204:239–250. doi:10.1016/S0927-7757(01)01138-4

Stukan MR, Ligneul P, Crawshaw JP, Boek ES (2010) Spontaneous imbibition in nanopores of different roughness and wettability. Langmuir 26:13342–13352. doi:10.1021/la101995t

Tartakovsky A, Meakin P (2005) Modeling of surface tension and contact angles with smoothed particle hydrodynamics. Phys Rev E 72:02630. doi:10.1103/PhysRevE.72.026301

Washburn EW (1921) The dynamics of capillary flow. Phys Rev 17:273–283. doi:10.1103/PhysRev.17.273

Weislogel MM, Baker JA, Jenson RM (2011) Quasi-steady capillarity-driven flows in slender containers with interior edges. J Fluid Mech 685:271–305. doi:10.1017/jfm.2011.314

Xiao Y, Yang F, Pitchumani R (2006) A generalised analysis of capillary flow in channels. J Colloid Interface Sci 298:880–888. doi:10.1016/j.jcis.2006.01.005

Xue HT, Fang ZN, Yang Y, Huang JP, Zhou LW (2006) Contact angle determined by spontaneous dynamic capillary. Chem Phys Lett 432:326–330. doi:10.1016/j.cplett.2006.10.017

Yang D, Krasowska M, Priest C, Popescu MN, Ralston J (2011) Dynamics of capillary-driven flow in open microchannels. J Phys Chem C 115:18761–18769. doi:10.1021/jp2065826

Yost F, Holm E (1995) Capillary flow on narrow strips and in V-shaped grooves. Advances in electronic packaging. In: Proceedings of INTERPACK'95 conference, ASME EEP, vol 10, pp 1265–1271

Zhu Y, Petkovic-Duran K (2010) Capillary flow in microchannels. Microfluid Nanofluid 8:275–282. doi:10.1007/s10404-009-0516-4